Topics in Catalysis (2023) 66:1020–1030
https://doi.org/10.1007/s11244-022-01719-x

ORIGINAL PAPER

Low-Temperature H_2-deNO$_x$ in Diesel Exhaust

Enno Eßer[1] · Kim Müller[1] · Sven Kureti[1]

Accepted: 10 October 2022 / Published online: 14 November 2022

Abstract
For NO$_x$ removal from diesel exhaust, the selective catalytic reduction (SCR) is the most common abatement technology. However, low engine load scenarios such as city driving and cold start phases demand efficient NO$_x$ reduction clearly below 200 °C, which is difficult to achieve with SCR. Hence, this work investigates the potential of the low-temperature NO$_x$ reduction with H_2 in diesel exhaust. A monolithic Pt/WO$_x$/ZrO$_2$ catalyst, recently reported as highly active, was evaluated in synthetic and real diesel exhaust. The monolith demonstrated high deNO$_x$ activity between 130 and 215 °C in the synthetic exhaust including peak conversion of 90% with N_2 selectivity up to 85%. CO/HC components were shown to inhibit the H_2-deNO$_x$ conversion thus requiring a pre-oxidation catalyst in practice. Furthermore, studies performed in an optical reactor indicated strong heat evolution along the monolith. As a result, the reaction kinetics was accelerated with an enhanced consumption of H_2 limiting the H_2-deNO$_x$ efficiency above 200 °C. Stationary tests in diesel engine exhaust substantiated the low-temperature H_2-deNO$_x$ performance of the monolith including NO$_x$ conversions up to 80% at temperatures as low as 135 °C.

Keywords NO$_x$ reduction · H_2 reductant · catalyst · exhaust gas aftertreatment · reaction zone · diesel exhaust

1 Introduction

Combustion engines are the most important propulsion systems for transportation but come increasingly under pressure due to the emission of CO_2 and pollutants. Thus, battery and fuel cell electric vehicles are intensely developed, whereas combustion engines will still be needed in the next decades to guarantee energy supply. Additionally, sustainable fuels based on biogenic and synthetic components are more and more advanced towards the substitution of fossil resources. Furthermore, exhaust gas after-treatment techniques were worldwide introduced to abate pollutants from combustion engines. For stoichiometric gasoline vehicles, three-way catalysts are employed, which simultaneously convert hydrocarbons (HC), carbon monoxide (CO) and nitrogen oxides (NO$_x$). For diesel exhaust, diesel oxidation catalysts (DOC) are taken to remove HC and CO, while particulate matter is separated by diesel particulate filters (DPF). Additionally, NO$_x$ [1] is widely eliminated by the selective catalytic reduction (SCR) employing V_2O_5/WO_3/TiO_2 [2] or Fe-/Cu-zeolite catalysts [3]. SCR uses NH_3 as reducing agent ($4\ NO + 4\ NH_3 + O_2 \rightarrow 4\ N_2 + 6\ H_2O$), which is produced on-board from urea, and operates between approx. 220 and 550 °C. However, its limited performance below 200 °C is increasingly an issue closely associated with the engine efficiency, which has been continuously enhanced in the recent years. In particular, low exhaust temperatures reflect engine cold start, city driving, stop-and-go traffic and intermittent operation of the combustion engine in hybrid vehicles. These operation ranges of diesel engines are challenging to meet latest emission limits demanding real driving scenarios. In this context, the reduction of NO$_x$ by hydrogen (H_2-deNO$_x$, Eq. 1) is known as a promising approach to remove nitrogen oxides at low temperatures, whereupon precious metal catalysts are known to be most active [4]. High H_2-deNO$_x$ efficiency below 200 °C was recently demonstrated for the first time in real diesel [5] and lean H_2 combustion engine exhaust using Pt catalysts [6]. Despite this progress towards practical application, crucial constraints remain including the side-production of N_2O (Eq. 2) [7] and competing consumption of H_2 by O_2 present in excess (Eq. 3). Nevertheless, the

✉ Sven Kureti
kureti@iec.tu-freiberg.de

[1] Institute of Energy Process Engineering and Chemical Engineering, Chair of Reaction Engineering, Technical University of Freiberg, Fuchsmühlenweg 9, 09599 Freiberg, Germany

H_2-deNO$_x$ reaction can be clearly enhanced by increasing the molar H_2/NO_x ratio. Additionally, the increased amount of H_2 heats up the catalyst due to the exothermic conversions (Eqs. 1–3) thus shifting the range of substantial H_2-deNO$_x$ activity to lower catalyst inlet temperatures [5].

$$2\,NO_{(g)} + 2\,H_{2\,(g)} \rightarrow N_{2\,(g)} + 2\,H_2O_{\,(g)} \quad \Delta H^\circ = -668\ kJ/mol \tag{1}$$

$$2\,NO_{(g)} + H_{2\,(g)} \rightarrow N_2O_{\,(g)} + H_2O_{\,(g)} \quad \Delta H^\circ = -342\ kJ/mol \tag{2}$$

$$O_{2\,(g)} + 2\,H_{2\,(g)} \rightarrow 2\,H_2O_{\,(g)} \quad \Delta H^\circ = -572\ kJ/mol \tag{3}$$

A comprehensive overview on effective H_2-deNO$_x$ catalysts under O_2-rich conditions was demonstrated in recent articles and reviews [8–12]. Promising catalysts investigated on the powder level are Pt/MgO-CeO$_2$ [13], Pd/LaCoO$_3$ [14] and Pt/WO$_3$/TiO$_2$ [15] revealing high activity below 200 °C with maximal NO$_x$ conversions above 80% and corresponding N_2 selectivities between 80 and 90%. Additionally, WO$_x$-promoted Pt/ZrO$_2$ showed NO$_x$ conversion of 98% at temperatures as low as 80 °C with N_2 selectivities up to 90% [16]. Different pathways of the H_2-deNO$_x$ reaction were reported in the literature. For Pt/WO$_x$/ZrO$_2$ [17] and Pt/SiO$_2$/Al$_2$O$_3$ [12], the platinum atoms are considered to act as the sole active site, on which NO dissociatively adsorbs followed by recombination of two N atoms to yield N_2, whereas N_2O originates from combination of N and NO adsorbates [18]. Moreover, for Pt/WO$_x$/SiO$_2$/Al$_2$O$_3$ [12] and Pt/W/HZSM-5 [19], NH$_x$ intermediates formed at the interface of Pt and the respective substrate were suggested to participate in a SCR-related reaction. Also, dissociation of H_2 on the Pt sites and migration of the formed H atoms to NO$_x$ surface species located on the substrate was proposed for Pt/MgO-CeO$_2$ [13].

The present article addresses the low-temperature H_2-deNO$_x$ conversion with special focus on the effect of CO and HC using a diesel engine test bench and a monolithic Pt/WO$_x$/ZrO$_2$ catalyst. For comprehensive understanding of the results gained in the diesel exhaust line, tests on a laboratory rig were performed including a model exhaust with defined CO and C_3H_6 proportions. Additional studies were made with an optical reactor to identify reaction zones inside the catalytic monolith upon H_2-deNO$_x$.

2 Experimental

2.1 Catalyst Preparation

The catalyst used in this study was a recently reported WO$_x$-promoted Pt/ZrO$_2$ catalyst developed for H_2-deNO$_x$ in lean H_2 combustion engines [5, 6]. For clarity, the preparation is briefly described here. The commercial ZrO$_2$ support was coated with the WO$_x$ promotor and the Pt active component by using the incipient wetness. A defined volume of a solution of $(NH_4)_6H_2W_{12}O_{40}\cdot H_2O$ (Honeywell) with known W content was dropwise added to the support such that it was completely absorbed. After drying at 80 °C, Pt was introduced in a very similar manner taking a solution of Pt(NO$_3$)$_2$ (Chempur). The sample was then dried overnight in air at 80 °C followed by activation at 300 °C for 180 min in a flow of 2.5 vol.% H_2 and 97.5 vol.% N_2 (heating rate: 2 K/min). Finally, the catalyst was calcined in static air at 500 °C for 5 h (heating rate: 1.7 K/min).

The powder catalyst was coated onto two monolithic honeycomb substrates (cordierite, 600 cpsi, 5.66″ × 3″) resulting in a catalyst load of 80 g/l each. The coating was processed by Umicore. For the H_2-deNO$_x$ tests in synthetic diesel exhaust, 1″ × 2″ cores were extracted from a honeycomb, while for the investigations in real diesel exhaust, the full-size monoliths were employed and fitted to a homemade metal housing (5.66″ × 6″). For the studies with the optical reactor, a recently reported monolithic Pt/WO$_x$/ZrO$_2$ model catalyst, also coated by Umicore, was used implying a 400 cpsi cordierite honeycomb and a loading of 100 g/l [16]. Cores with a 1.4 × 1.4 cm square base and lengths between 1.2 and 6 cm were taken from the full size brick.

2.2 Catalyst Characterization

N_2 physisorption was performed on a TriStar II (Micrometrics). Prior to the analyses, respective sample was outgassed in vacuum (10^{-1} mbar, 16 h) at 350 °C to remove adsorbed species such as H_2O. The BET surface area (S_{BET}) was obtained from adsorption data at -196 °C and p/p_0 ratios between 0.05 and 0.20.

Temperature-programmed desorption of CO (CO-TPD) was used to quantify the available Pt sites of the catalyst powder. A sample mass of 200 mg was charged into a U-shaped glass reactor [20] and pretreated for 15 min at 500 °C in 5 vol.% O_2 (He balance) to remove adsorbed species. At the same temperature, the sample was flushed with He and then exposed to a mixture of 3000 ppm CO and He (balance) for 15 min to reduce the Pt surface. After this, it was cooled to -196 °C in flowing He and the sample was saturated with CO by dosing a blend of 750 ppm CO and He (balance). The low adsorption temperature was taken to avoid spill-over of CO from the Pt sites to the support as previously reported for similar catalysts [21, 22]. Subsequently, it was flushed with He until no more CO was detected in the gas phase. Note that for all these steps, the total gas flow was kept at 400 ml/min (STP). Finally, the TPD was started by increasing the temperature at a rate of 20 K/min while supplying a He flow of 150 ml/min (STP). The temperature

was recorded by a K-type thermocouple inside the sample in middle of the sample chamber through a notch in the reactor. Gaseous CO and CO_2 were continuously monitored by non-dispersive infrared spectroscopy (NDIR, X-Stream Enhanced XEGK, Emerson). It should be mentioned that in TPD CO, which desorbs below 100 °C, is originated from the support as shown by blank experiments made with the bare support. Additionally, above approx. 100 °C CO desorbing from the Pt sites is totally converted into CO_2 by subsequent reaction with the support. This supposition is in line with the literature [23, 24] and was confirmed by the blank experiments indicating only minor desorption of CO_2 from the bare support. Thus, for the determination of the available Pt sites, the CO_2 signal detected in TPD was integrated and the contribution of the minor CO_2 signal of the blank TPD was subtracted. With the resulting molar amount of CO_2 and assuming a CO/Pt stoichiometry of 1 [25] the total number of available Pt sites (n_a(Pt)) was derived. The dispersion of Pt (D_{Pt}) was calculated from n_a(Pt) and the total number of Pt atoms (n_{Pt}) known from the incipient wetness impregnation ($D_{Pt} = n_a(Pt)/n_{Pt}$). The mean Pt particle size (d_{Pt}) was estimated by supposing perfect spheres, i.e. $d_{Pt} = 6V_{Pt}/(a_{Pt} \cdot D_{Pt})$, whereas V_{Pt} is the volume of a Pt atom in the bulk (15.10 $Å^3$) and a_{Pt} represents the surface area of a Pt atom located on a polycrystalline surface (8.07 $Å^2$) [25]. All samples were characterized in powder form prior to deposition on the monolith.

2.3 Catalytic Studies

2.3.1 Experiments with the Laboratory Test Bench and the Optical Reactor

The catalytic H_2-deNO$_x$ investigations in the diesel model exhaust gas were performed on a laboratory test bench using the 1″ × 2″ cores. Respective monolith was placed in the tubular quartz glass reactor slightly larger than the honeycomb catalysts, heated by an external oven, and was wrapped by quartz wool to avoid bypassing. Temperatures were recorded by K-type thermocouples located directly in front of and behind the honeycomb. The gases were dosed by independent mass flow controllers (Bronkhorst) at a total flow of 17.1 l/min (STP) resulting in a space velocity of 40,000 h^{-1}. The model exhaust was composed of y(NO) = 200 ppm, y(H_2) = 4000 ppm, y(CO) = 150 ppm, y(C_3H_6) = 50 ppm, y(H_2O) = 4.5 vol.%, y(CO_2) = 4.8 vol.% and y(O_2) = 13.8 vol.%, (N_2 balance). Before the H_2-deNO$_x$ tests, the catalyst was heated to 300 °C in air, the model exhaust was adjusted, while linearly decreasing the temperature to 100 °C at the rate of 1.7 K/min. Preliminary investigations using this method have revealed a quasi-stationary catalyst behavior. The simultaneous analysis of NO, NO_2, N_2O, NH_3, CO, CO_2, C_3H_6 and H_2O was carried out by a hot measuring online FTIR spectrometer (Multi-Gas Analyzer 2030, MKS Instruments), whereas O_2 was continuously monitored by a lambda probe (LSU 4.9, Bosch). The H_2 flow was checked before the H_2-deNO$_x$ tests by using a special pipe system of the bench equipped with a dedicated oxidation catalyst and defined O_2/N_2 supply. With this catalyst the dosed H_2 was completely converted into H_2O, which was detected.

For the assessment of the H_2-deNO$_x$ performance, the conversion of NO$_x$ [$X(NO_x) = 1 - y(NO_x)_{out}/y(NO_x)_{in}$] and selectivity of N_2O [$S(N_2O) = 2\ y(N_2O)/(y(NO_x)_{in} - y(NO_x)_{out})$] were used. The latter is exclusively presented for NO$_x$ conversions above 20% to minimize error propagation. As N_2 was not directly measured, its selectivity was calculated from that of N_2O [$S(N_2) = 1 - S(N_2O)$]. Its formation in H_2-deNO$_x$ has been shown in previous experiments by GC/TCD analysis using Ar as balance [16].

The laboratory facility with the optical reactor was used to investigate reaction zones inside the monolith by measuring the local heat temperature. The reactor consists of CaF_2, which is permeable for UV/VIS and IR radiation, and reveals a square base of 1.4 × 1.4 cm with a height of 9 cm. The temperature was adjusted by an oven placed in front of the CaF_2 reactor, whereas reference temperatures were taken by K-type thermocouples located directly in front of and behind the monolith, which was introduced into the optical reactor. The thermal imaging camera PYROVIEW 380 M (DIAS Infrared) was positioned close to the optical reactor such that the whole length of the monolith was scanned. The camera collected a spectral range from 3 to 5 µm corresponding to temperatures between 100 and 300 °C, whereas the thermal images were recorded and processed using the software PYROSOFT Compact. Supply and analysis of the gases were conducted as in the laboratory tests described above. The total flow was 3 l/min (STP) and constant inlet temperatures between 105 and 165 °C were adjusted. After reaching the desired temperature in a gas flow consisting of 5 vol.% O_2 in N_2, the reactive gases (y(NO) = 2000 ppm, y(H_2) = 6000 ppm) were added and thermal images were recorded after reaching a stationary temperature profile. In the H_2-deNO$_x$ investigations, the length of the monolith was varied between 1.2 and 6.0 cm corresponding to space velocities from 18,000 to 90,000 h^{-1}. While the NO$_x$ conversion was determined as described above the H_2 conversion was calculated from the H_2O proportion monitored by the FTIR analyzer [$X(H_2) = 1 - y(H_2O)_{out}/y(H_2)_{in}$].

2.3.2 Experiments on the Diesel Engine Test Bench

The H_2-deNO$_x$ investigations in diesel exhaust were performed by employing an emergency power generator (YTO YD385D, Yangdong) with an engine displacement of 1.5 l and a maximal power output of 11 kW providing an exhaust

stream of approx. 880 l/min (STP). The exhaust line consisted of a commercial cordierite-based diesel oxidation catalyst (DOC, 5.66″ × 3″, 400 cpsi, precious metal loading: 30 g/ft³, Pt/Pd mass ratio: 6:1), a commercial DPF (SiC, HJS Technologies), an exhaust cooler and the monolithic H_2-deNO$_x$ catalyst. The DOC was positioned close to the engine to achieve CO and HC light-off (approx. 200 °C) removing all carbon containing pollutants. The pressure loss of the particulate filter was continuously monitored (IDPS 200, Schneider Messtechnik), whereas filter regeneration was performed before each H_2-deNO$_x$ experiment by using an external oven (550 °C, 4 h, static air). The exhaust cooling was made with a gas recirculation cooler (Scania) designed for truck engines enabling stationary inlet temperatures at the H_2-deNO$_x$ catalyst between 100 and 180 °C. The required H_2 was dosed by a mass flow controller (Bronkhorst) and was injected centrally counter-streamwise behind the particulate filter. A butterfly mixer [26] was used to homogenize the H_2 distribution in the gas stream. Prior to the H_2-deNO$_x$ experiments, the exhaust compositions were checked by the FTIR analyzer and lambda probe described above. During the tests, the NO$_x$ proportions were recorded by NO$_x$ probes (UniNO$_x$, Continental) placed in front of and behind the H_2-deNO$_x$ catalyst. The H_2 fractions present in the exhaust gas after the H_2-deNO$_x$ catalyst were checked by online gas chromatography coupled with thermal conductivity detection (GC/TCD INFICON 3000 Micro GC, Inficon). The exhaust temperature was continuously monitored in front of and behind each aftertreatment device by K-type thermocouples.

3 Results and Discussion

3.1 Catalyst Properties

The Pt/WO$_x$/ZrO$_2$ sample prepared to washcoat the honeycomb substrates was the same as reported earlier and displays a very similar H_2-deNO$_x$ performance and catalyst properties [5]. The most important physico-chemical properties of the catalyst powder are briefly summarized in Table 1.

Table 1 BET surface area (S_{BET}), number of available Pt sites (n_a(Pt)), Pt dispersion (D(Pt)) and estimated Pt particle size (d(Pt)) of the catalyst powder

Pt content [wt.%]	S_{BET} [m²/g]	n_a(Pt) [a] [µmol/g]	D(Pt) [b] [%]	d(Pt) [c] [nm]
0.25	95	12	91	1.2

[a]Obtained from CO-TPD

[b]$D_{Pt} = n_a(Pt) / n_{Pt}$

[c]$d_{Pt} = 6\ V_{Pt} / (a_{Pt}\ D_{Pt})$

In accordance with a recent study on related Pt/WO$_x$/SiO$_2$/Al$_2$O$_3$ catalysts, a key feature driving the H_2-deNO$_x$ activity is the high Pt dispersion [12], which was indeed achieved for Pt/WO$_x$/ZrO$_2$. As a consequence, the Pt loading of the coated monoliths amounted to approx. 6 g/ft³ only, which is a very low precious metal content compared to state-of-the-art diesel oxidation catalysts and three-way catalysts.

3.2 Effect of CO and HC on H_2-deNO$_x$ in Synthetic Diesel Exhaust

The effect of CO and HC on the low-temperature H_2-deNO$_x$ conversion was investigated under conditions mimicking city driving of a diesel passenger car. This scenario is reflected by low engine load resulting in exhaust temperatures below 200 °C, low fractions of H_2O/CO_2 and relatively high proportions of O_2 [5]. For these investigations, the 1″ × 2″ monolith was used, while adjusting a H_2 fraction of 4000 ppm corresponding to a $y(H_2)/y(NO_x)$ ratio of 20, which was recently shown to provide substantial H_2-deNO$_x$ [5]. The proportions of H_2O, CO_2 and O_2 were 4.5 vol.%, 4.8 vol.% and 13.8 vol.% in line with the city driving conditions. In a benchmarking test, a synthetic diesel exhaust without HC/CO was adjusted assuming an active DOC placed in front of the H_2-deNO$_x$ stage. The resulting H_2-deNO$_x$ performance (Fig. 1) showed NO$_x$ conversions of more than 90% in the low-temperature regime including a N_2 selectivity up to 85%. The temperature window for significant NO$_x$ reduction lay between 130 and 215 °C. However, outside of this optimal operation range, the N_2O selectivity increased significantly reaching up to 50%. On the contrary, NH_3 formation was not observed at all.

For the scenario without active pre-DOC, proportions of CO (150 ppm) and HC were additionally adjusted using

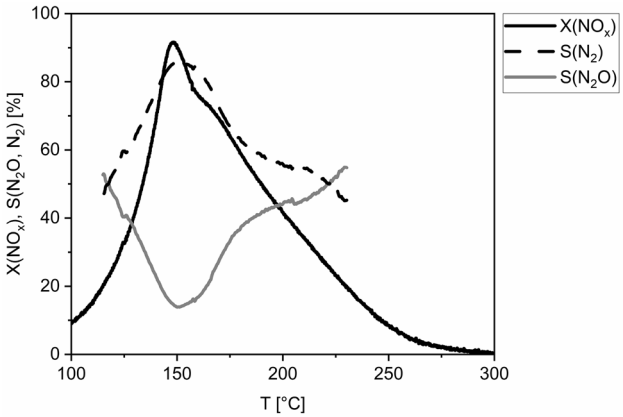

Fig. 1 H_2-deNO$_x$ performance of the 1″ × 2″ monolith (600 cpsi, 80 g/l) in diesel model exhaust without CO/HC. Reaction conditions: y(NO) = 200 ppm, $y(H_2)$ = 4000 ppm, $y(H_2O)$ = 4.5 vol.%, $y(CO_2)$ = 4.8 vol.%, $y(O_2)$ = 13.8 vol.%, N_2 balance, GHSV: 40,000 h^{-1}

C_3H_6 as model HC (50 ppm). These concentrations were reported for city traffic simulations, whereas the dosed amount of C_3H_6 corresponds to the C1 equivalent of total HC [5]. Figure 2 evidences strongly decreasing H_2-deNO$_x$ efficiency in the presence of CO/HC compared to the study without supply of CO/HC. In particular, the maximal NO$_x$ conversion declined to approx. 30% at 145 °C, while only minor NO$_x$ reduction occurred below 125 °C. Additionally, the maximal selectivity towards N_2 decreased from 85 to 70%. Total CO conversion was observed at temperatures above 140 °C and C_3H_6 was entirely oxidized at temperatures higher than 165 °C.

To identify the individual effects of CO and C_3H_6 H_2-deNO$_x$ studies with each component were conducted separately. As shown in Fig. 3, the addition of 150 ppm CO (without C_3H_6) to the synthetic model exhaust had a strong effect on the H_2-deNO$_x$ reaction leading to complete loss of activity below 125 °C but having no effect on the NO$_x$ reduction above 140 °C decreasing the maximal N_2 selectivity only slightly from 85 to 75%. Additionally, the light-off temperature of the H_2-deNO$_x$ reaction (125–140 °C) correlates with the light-off temperature of the CO oxidation. Therefore, the loss of low-temperature activity in the presence of CO and C_3H_6 is attributed to the presence of CO in the exhaust gas but is not involved in the reduced H_2-deNO$_x$ activity above the CO light-off temperature. This finding is in line with literature attributing the loss of low-temperature efficiency to the blockage of active Pt sites by CO, while at temperatures above the light-off temperature of CO sufficient Pt sites are available for simultaneous NO$_x$ reduction and CO adsorption and oxidation [16, 27].

The sole presence of 50 ppm C_3H_6 (without CO) in the exhaust gas led to a significantly decreased H_2-deNO$_x$ activity in the whole temperature range (Fig. 4). The maximal NO$_x$ conversion of approx. 60% was observed at 125 °C with a significant N_2O selectivity of more than 30%. In contrast to the experiments with only CO, no clear correlation between C_3H_6 light-off temperature and H_2-deNO$_x$ activity becomes apparent. Incomplete C_3H_6 oxidation to CO was not detected. Similar to the experiments with CO supply, the reduced H_2-deNO$_x$ activity is attributed to the blockage of active Pt sites by C_3H_6 or its intermediate species [28] occurring during conversion to CO_2 and H_2O.

From the above tests investigating the effect of CO and HC it is inferred that an active DOC positioned in front of the H_2-deNO$_x$ stage is mandatory for practice, since CO and HC strongly inhibit the NO$_x$ reduction, particularly at low temperatures. Thus, the H_2-deNO$_x$ studies made in real

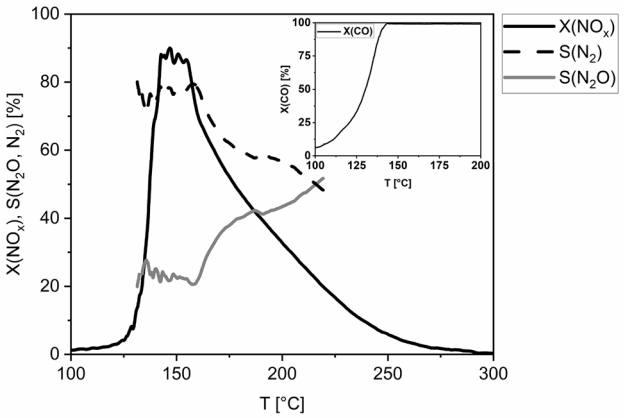

Fig. 3 H_2-deNO$_x$ performance of the 1″ × 2″ monolith (600 cpsi, 80 g/l) in diesel model exhaust with CO. Reaction conditions as stated in Fig. 1 with additional y(CO) = 150 ppm. The CO conversion is shown in the inset

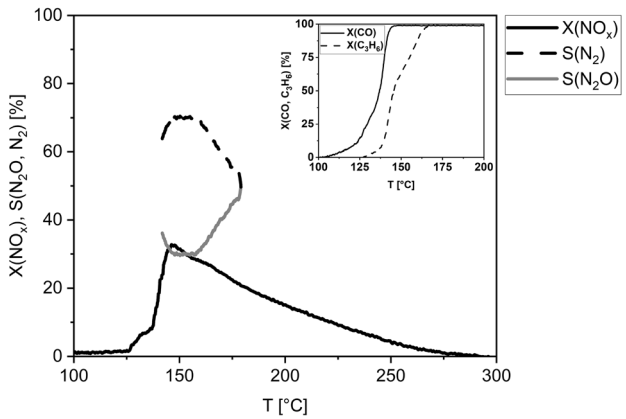

Fig. 2 H_2-deNO$_x$ performance of the 1″ × 2″ monolith (600 cpsi, 80 g/l) in diesel model exhaust with CO/HC. Reaction conditions as stated in Fig. 1 with additional y(CO) = 150 ppm and y(C_3H_6) = 50 ppm. The respective CO and C_3H_6 conversions are shown in the inset

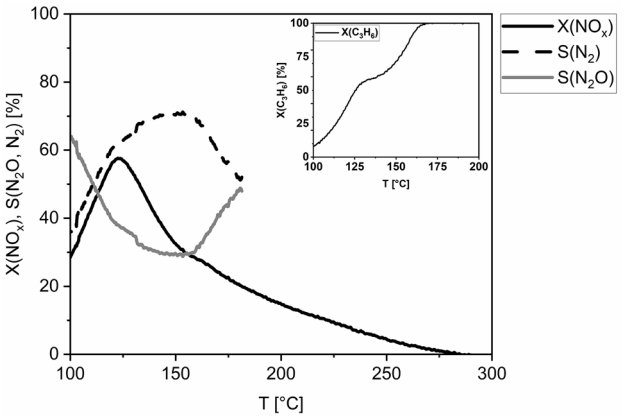

Fig. 4 H_2-deNO$_x$ performance of the 1″ × 2″ monolith (600 cpsi, 80 g/l) in diesel model exhaust with C_3H_6. Reaction conditions as stated in Fig. 1 with additional y(C_3H_6) = 50 ppm. The C_3H_6 conversion is shown in the inset

diesel exhaust were conducted with a commercial pre-DOC as shown in Sect. 3.4.

3.3 Evaluation of Reaction Zones Inside the Catalyst

Since the H_2-NO_x and H_2-O_2 conversions (Eqs. 1–3) are strongly exothermic, hot areas inside the catalyst can be formed potentially causing local auto-acceleration of the reactions. Thus, temperature profiles inside the catalyst were evaluated to identify such reaction zones. For this purpose, the optical reactor was used allowing the measurement of surface temperatures along the outer catalyst channels. These fundamental studies were performed with the monolithic Pt/WO_x/ZrO_2 model catalyst, as for this sample an elementary kinetic model is available [17, 29]. To investigate the effect of NO on the heat evolution and formation of reaction zones a monolith with a length of 6 cm (GHSV: 18,000 h^{-1}) was taken, while dosing a gas mixture of 0 or 2000 ppm NO, 6000 ppm H_2, 5 vol.% O_2 and N_2 as balance. The thermal images were taken under stationary conditions adjusting gas inlet temperatures between 105 and 165 °C (Fig. 5). In the absence of NO, the H_2 oxidation started at an inlet temperature of 125 °C as indicated by a temperature increase by 30 °C at the central upstream part of the monolith. With inclining inlet temperature, the reaction zone increasingly ranges over the entire width of the monolith, while the largest axial extension was 2.0 cm for the inlet temperature of for 165 °C resulting in a rise of 40 °C up to 205 °C (Fig. 5.) Note that for all inlet temperatures the strongest heat evolution, corresponding to the highest rate of H_2 oxidation, occurred at the central front side of the monolith. Contrary, the presence of NO shifted the H_2 light-off to higher temperature (approx. 145 °C) with a temperature rise of 25 °C while also shortening the axial extension of the reaction zone, e.g. from 1.8 cm to 1.4 cm at the catalyst inlet temperature of 155 °C. Also, the maximal temperature detected at a catalyst inlet temperature of 165 °C was only 195 °C indicating an inhibiting effect of NO on the H_2 oxidation. This is in line with the elementary kinetics of the lean H_2-deNO_x reaction showing predominant coverage of the Pt sites by NO below 200 °C. As a consequence, the adsorption and reaction of H_2 on the catalyst is limited thus shifting the H_2 oxidation to higher temperatures [17, 29].

Furthermore, the influence of the length of the monolith (1.2 cm, 3 cm, 6 cm) on the temperature profile upon H_2-deNO_x reaction was investigated retaining the total flow as well as gas composition. Note that the different lengths correspond to space velocities ranging from 18,000 h^{-1} to 90,000 h^{-1}. NO_x and H_2 conversions were again determined using the NO_x and H_2O proportions at the reactor outlet taken by the FTIR spectrometer. As a result, the thermal images (Fig. 6) show higher temperatures the shorter the monoliths are. For instance, at the inlet temperature of approx. 145 °C using a monolith with 6 cm a maximal temperature of ca. 170 °C appeared, while for the samples with 3 and 1.2 cm length temperature rose to 180 and 190 °C, respectively. The differences are attributed to heat transport by thermal conduction and convection as well as the heat capacity, which increases with catalyst mass and length, respectively. Heat conduction predominates in the laminar flow regime of the honeycomb (Re ≈ 150), whereas the heat transport from the catalyst to

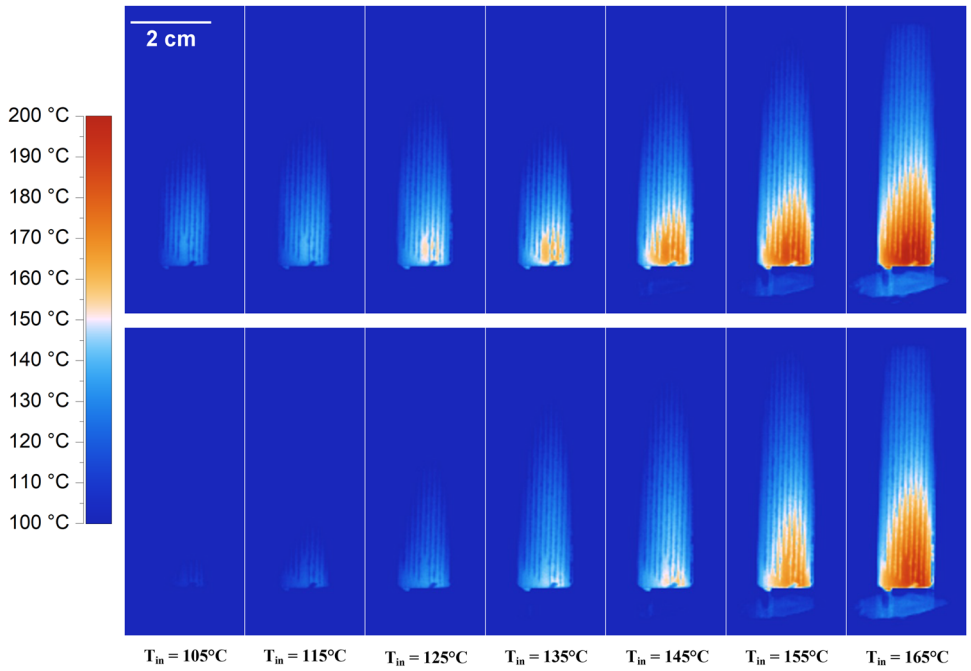

Fig. 5 Temperature distribution on the surface of the cuboid monolith (400 cpsi, 100 g/l, 1.4 × 1.4 × 6 cm, upward flow direction) in model exhaust with (bottom) and without NO (top) at gas inlet temperatures between 105 and 165 °C. Reaction conditions: y(NO) = 0 or 2000 ppm, y(H_2) = 6000 ppm, y(O_2) = 5 vol.%, N_2 balance, GHSV: 18,000 h^{-1}

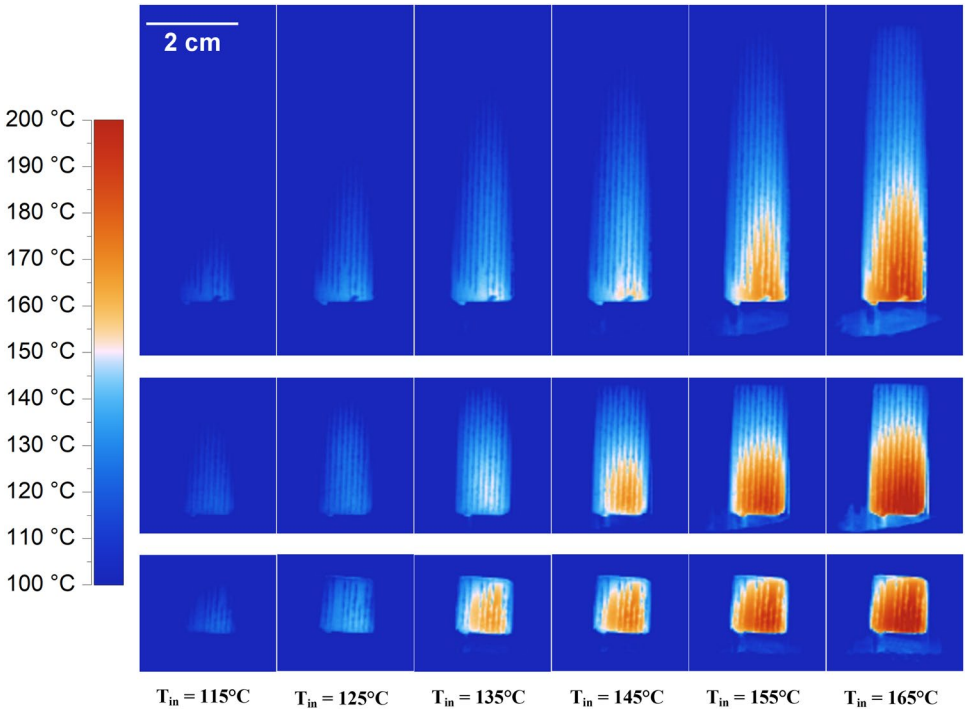

Fig. 6 Temperature distribution on the surface of the cuboid monoliths (400 cpsi, 100 g/l, 1.4 × 1.4 cm, upward flow direction) with lengths of 1.2 cm (bottom), 3 cm (middle) and 6 cm (top) in model exhaust at gas inlet temperatures between 115 and 165 °C. Reaction conditions: y(NO) = 2000 ppm, $y(H_2)$ = 6000 ppm, $y(O_2)$ = 5 vol.%, N_2 balance, GHSV: 18,000–90,000 h^{-1} (lower images)

the environment directly correlates with the contact area [30]. As with reducing the length from 6 to 1.2 cm the surface area of the cuboid honeycomb is lowered from 321 to 64 cm^2, it is clear that the heat transition from the monolith to the surroundings is drastically lowered. It should be mentioned that the heat conductivity of the solid fraction of the catalyst is higher compared to the gas flow as indicated by the thermal conductivity coefficients (k), which amount to 1.3–2.5 W/mK for cordierite, 1.5–2 W/mK for ZrO_2 as the main washcoat component, but only 0.02 W/mK for N_2 as the main gas component [31]. Additionally, the heat capacity of the honeycomb is substantially decreased when using the shorter monoliths, which consequently take up less heat. For instance, the heat capacity of the 1.2 cm honeycomb is only 20% of that with 6 cm length due to its lower mass. As a result of the reduced heat transfer and heat capacity of the shorter catalysts, the temperature is increased inside the catalyst accelerating the H_2 oxidation and shifting the light-off temperature to lower inlet temperatures as shown in Fig. 7.

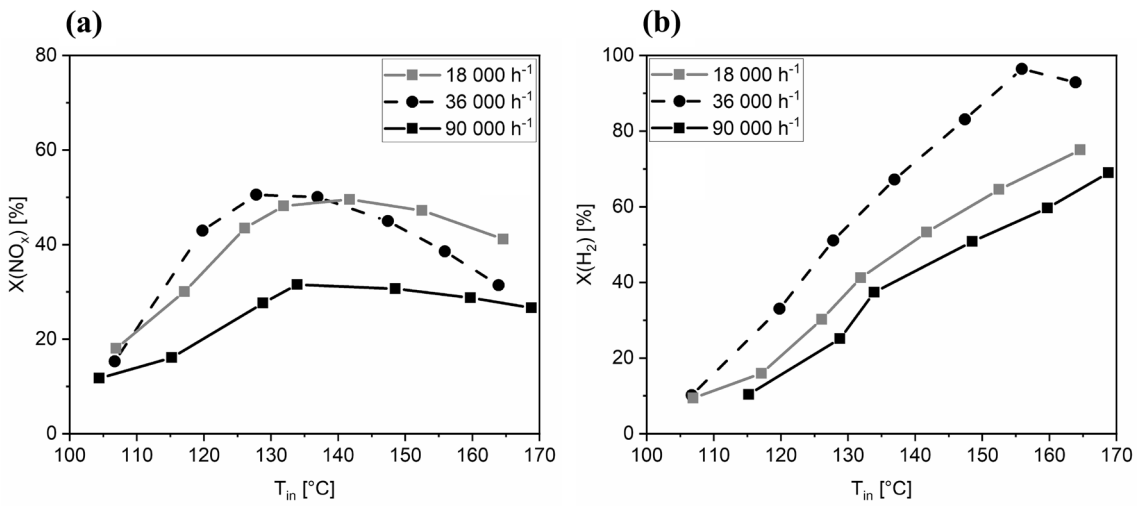

Fig. 7 Conversion of NO_x **a** and H_2 **b** in the H_2-deNO_x reaction on the cuboid monoliths (400 cpsi, 100 g/l, 1.4 × 1.4 cm) with lengths of 1.2 (90,000 h^{-1}), 3 (36,000 h^{-1}) and 6 cm (18,000 h^{-1}) at gas inlet temperatures between 115 and 165 °C using the model exhaust stated in Fig. 6

Moreover, Figs. 5 and 6 demonstrate a parabolic radial distribution of the temperature inside the monoliths. This effect is obviously related to the heat transfer from the centre of the honeycomb to the environment of the optical reactor. This cooling effect is very likely supported by the gas, which flows in the outer catalyst channels along the edges of the reactor. Since no catalytic reaction takes place on the walls and no backmixing occurs inside the gas stream due to the laminar flow regime, the gas streaming at the edges acts as a cooling film and so it enhances the radial temperature distribution.

The influence of the different temperature profiles on the H_2-deNO$_x$ reaction at different space velocities becomes apparent when comparing the corresponding NO$_x$ and H_2 conversions (Fig. 7). The shift of NO$_x$ conversions to lower temperatures when shortening the catalyst from 6 to 3 cm, hence increasing the GHSV from 18,000 to 36,000 h^{-1}, corresponds to the higher temperatures of the monolith accelerating the H_2-deNO$_x$ reaction. Additionally, the H_2-O_2 conversion, which is more temperature sensitive than the H_2-deNO$_x$ reaction due to its faster reaction kinetics [17], increases more strongly than the NO$_x$ conversion; for instance at the inlet temperature of 125 °C the H_2 conversion inclines from 30% (18,000 h^{-1}) to 50% (36,000 h^{-1}), while the NO$_x$ conversion only grows from approx. 40 to 50%. When increasing the space velocity even higher from 36,000 to 90,000 h^{-1} by shorting the catalyst from 3 to 1.2 cm the NO$_x$ conversion as well as H_2 conversion clearly decrease for all inlet temperatures. As the reaction zone for the H_2-deNO$_x$ reaction is within the first 2 cm of the monolith according to the thermal images (Fig. 6), this decrease in catalytic activity is attributed to the lower residence time (τ) inside the monolith with a length of only 1.2 cm (τ(l = 1.2 cm) = 47 ms, τ(l = 6 cm) = 235 ms). The fraction of H_2 taking part in the H_2-deNO$_x$ reactions (Eqs. 1 and 2) reaches up to 50% at temperatures of highest NO$_x$ conversion, i.e. between 125 and 135 °C. However, above 135 °C the proportion of H_2 reacting with O_2 (Eq. 3) is strongly increased and at catalyst inlet temperatures above 160 °C this fraction exceeds 80% similar to reports on other H_2-deNO$_x$ catalysts [8, 10, 32].

3.4 H_2-deNO$_x$ Efficiency in Real Diesel Exhaust

The potential of the low-temperature H_2-deNO$_x$ efficiency in real diesel exhaust was evaluated with the two consecutive 5.66″ × 3″ monoliths by systematically varying the H_2 supply. The H_2-deNO$_x$ catalyst was positioned downstream to the DOC, the particulate trap and the exhaust cooler. The engine was operated stationarily at constant engine speed resulting in a space velocity of 22,000 h^{-1} mimicking city driving and stop-and-go traffic. The air-fuel ratio was set to $\lambda = 2.4$ ($y(H_2O) = 5.7$ vol.%, $y(CO_2) = 6$ vol.%, $y(O_2) = 12.0$ vol.%) and $\lambda = 1.9$ ($y(H_2O) = 7.1$ vol.%, $y(CO_2) = 7.5$ vol.%, $y(O_2) = 10.0$ vol.%) by adjusting the load to approx. 60% and 85% respectively. The temperature at the H_2-deNO$_x$ catalyst inlet was adjusted by the exhaust cooler to below 200 °C typical for cold start conditions.

In the tests using an air-fuel ratio of $\lambda = 2.4$ the maximal NO$_x$ conversion clearly increased from approx. 5 to 60% when raising the H_2 fraction from 1000 ppm to 1 vol.% (Fig. 8). This finding was expected from previous studies [5, 17] showing enhanced H_2-deNO$_x$ by increasing availability of hydrogen on the active Pt sites of the catalyst. Simultaneously, the temperature of the maximal NO$_x$ conversion decreased from 165 to 145 °C. This is associated with the heating of the monoliths due to the exothermic H_2-O_2 reaction accelerating with growing H_2 fraction. Such heat evolution inside the monoliths has been shown by the investigations with the optical reactor (Figs. 5 and 6) and is substantiated by the strongly increasing outlet temperatures, referred to the inlet, exemplarily rising by approx. 80 °C for 1 vol.% H_2 (Fig. 9b). As for the temperature of the maximal NO$_x$ conversion, the heat development in the catalyst also caused a shift of the light-off temperature of the H_2 oxidation to lower inlet temperatures (Fig. 9a). For instance, in the experiment with 5000 ppm H_2, the GC-TCD analysis indicated almost total conversion of H_2 at 155 °C, while with 1 vol.% full consumption already occurred at 145 °C.

However, the H_2-deNO$_x$ investigations showed continuous decrease in the NO$_x$ conversion when the inlet temperature exceeds 150 °C regardless of the proportion of H_2 (Fig. 8). This effect is related to the consumption of H_2 by the competing reaction with O_2, which is accelerated faster with increasing temperature than the NO reduction in agreement with the elementary kinetics of lean H_2-deNO$_x$ on Pt/

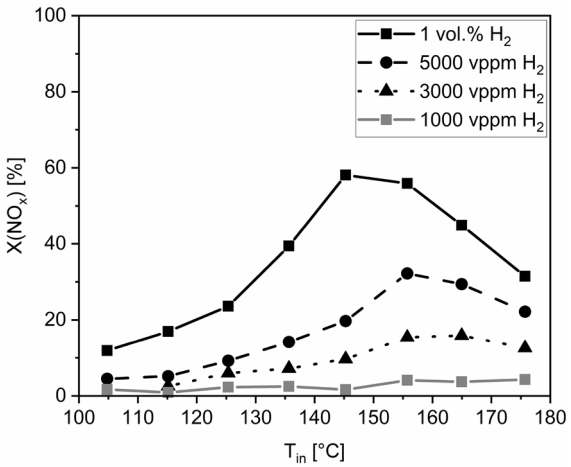

Fig. 8 H_2-deNO$_x$ performance of the two consecutive 5.66″ × 3″ monoliths (600 cpsi, 80 g/l) in diesel exhaust using an air-fuel ratio of $\lambda = 2.4$, a pre-DOC and DPF. Reaction conditions: $y(NO_x) = 500$ ppm, $y(H_2) = 1000$–10,000 ppm, $y(H_2O) = 5.7$ vol.%, $y(CO_2) = 6.0$ vol.%, $y(O_2) = 12.0$ vol.%, N_2 balance, GHSV: 22,000 h^{-1}

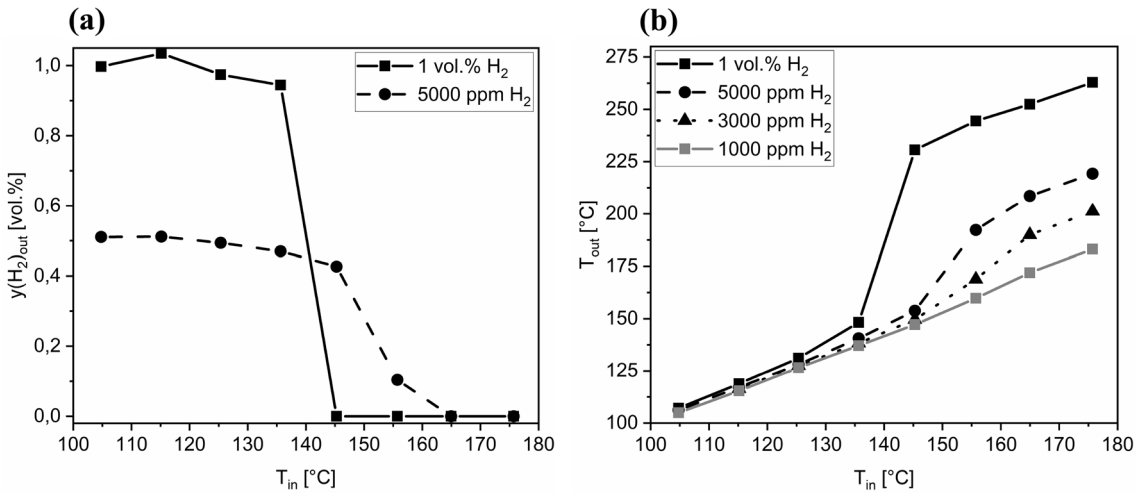

Fig. 9 H_2 fraction **a** and outlet temperatures **b** of the two consecutive 5.66″ × 3″ monoliths (600 cpsi, 80 g/l) in diesel exhaust using an air-fuel ratio of λ = 2.4, a pre-DOC and DPF. Reaction conditions as stated in Fig. 8

WO_x/ZrO_2 [17]. Consequently, the H_2 availability for the reduction of NO_x is progressively diminished with temperature thus limiting the operation window of the H_2-deNO_x conversion.

In the tests using an air-fuel ratio of λ = 1.9 (Fig. 10) significantly higher NO_x conversions between 35% ($y(H_2) = 2000$ ppm)) and 80% ($y(H_2) = 1$ vol.%) were observed in comparison to experiments at λ = 2.4 (Fig. 8). This is attributed to the lower O_2 content decreasing the H_2 oxidation rate thus increasing the amount of hydrogen available for the NO_x reduction [17]. However, it is noteworthy that the increase in the H_2 proportion from 0.5 to 1 vol.% had only very little effect on the maximal NO_x conversion, which is explained by the heat evolution inside the monoliths increasing the outlet temperature from 135 °C at the inlet to 215 °C at the outlet for 1 vol.% H_2 and hereby shifting the catalyst outside the optimal H_2-deNO_x operation temperature.

4 Conclusion

The potential of the low-temperature NO_x reduction using H_2 as reducing agent (H_2-deNO_x) was investigated in diesel engine exhaust. The low-temperature range (< 200 °C) is of particular relevance for cold start and city driving scenarios, which are increasingly important to cover real driving emissions. A monolithic Pt/WO_x/ZrO_2 catalyst, recently

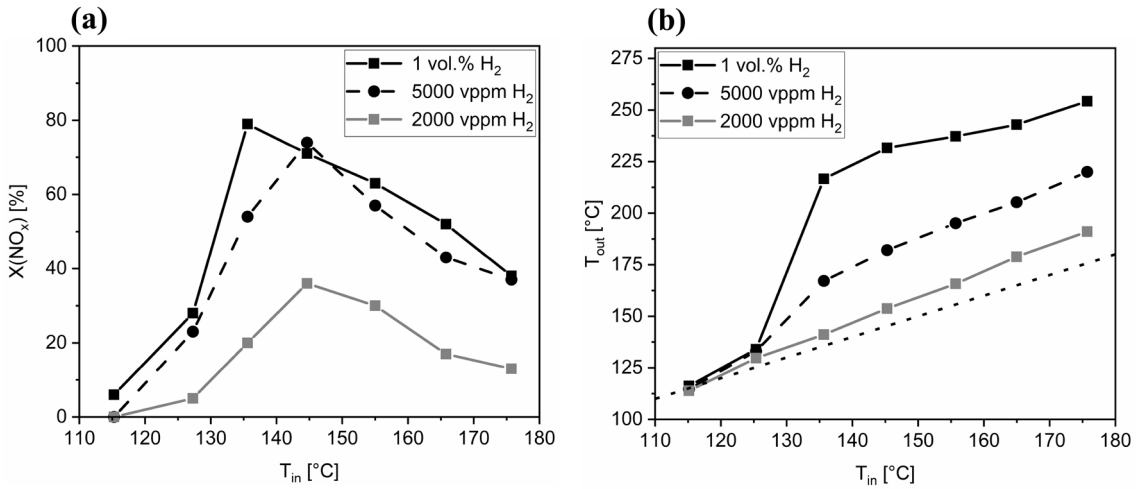

Fig. 10 H_2-deNO_x performance **a** and outlet temperatures **b** of the two consecutive 5.66″ × 3″ monoliths (600 cpsi, 80 g/l) in diesel exhaust using an air-fuel ratio of λ = 1.9, a pre-DOC and DPF. Reaction conditions: $y(NO_x) = 650$ ppm, $y(H_2) = 2000$–10,000 ppm, $y(H_2O) = 7.1$ vol.%, $y(CO_2) = 7.5$ vol.%, $y(O_2) = 10.0$ vol.%, N_2 balance, GHSV: 22,000 h^{-1}

shown as highly active, was firstly evaluated in synthetic diesel exhaust in form of a 1'' core and was then tested on the level of two consecutive 5.66″ × 3″ bricks in real diesel engine exhaust.

High NO_x conversions between 130 and 215 °C with maximal conversion of more than 90% and N_2 selectivity up to 85% were achieved in the model exhaust, whereas CO and HC strongly inhibited the H_2-deNO_x reaction due to competing adsorption and blocking of active Pt sites. Thus, an active pre-DOC is mandatory to keep the low-temperature efficiency of the H_2-deNO_x catalyst.

Stationary tests in real diesel engine exhaust using full-sized bricks substantiated the high H_2-deNO_x performance under city driving conditions including NO_x conversions up to 80% at temperatures as low as 135 °C. Simultaneously the exhaust gas temperature was increased up to 80 °C by the strongly exothermic H_2-O_2 and H_2-NO_x reactions. In future applications, this effect might be used to heat up the SCR stage, preferentially positioned downstream to the H_2-deNO_x unit, to enhance the SCR conversion. It might be speculated that such a faster SCR light-off can reduce the H_2 demand, particularly during cold start phases, since the H_2 is only required for the NO_x reduction at low exhaust temperatures. Therefore, the combination of conventional SCR with H_2-deNO_x seems highly promising for substantial NO_x reduction at all engine operating scenarios and should be investigated in further studies.

From experiments in an optical reactor, the catalyst inlet is identified to be the main reaction zone during H_2-deNO_x giving the opportunity for further catalyst optimization. Generally, this concept of a combined H_2-deNO_x catalyst with a downstream SCR unit may be useful for other lean combustion engines as well such as gas engines and H_2 engines having the potential to keep the NO_x output within future emission limits. However, further catalyst development remains necessary to lower the N_2O selectivity for all engine operation points.

Acknowledgements The authors thankfully acknowledge Umicore AG for catalyst coating and supply of the diesel oxidation catalysts as well as Keyou GmbH for granting permission to use their H_2-deNO_x catalyst technology. Furthermore, we would like to thank HJS Emission Technology GmbH & Co. KG for providing the diesel particulate filter.

Funding Open Access funding enabled and organized by Projekt DEAL.

Declarations

Conflict of interest The authors have no competing interest to declare that are relevant to the content of this article.

References

1. Air quality in Europe - 2019 report (2019) European Environment Agency, Copenhagen. www.eea.europa.eu. Accessed 23 June 2022
2. Koebel M, Elsener M, Marti T (1996) Combust Sci Technol 121:1–685
3. Kamasamudram K, Currier NW, Chen X, Yezerets A (2010) Catal Today 151:3212–3222
4. Shelef M, Jones JH, Kummer JT, Otto K, Weaver EE (1971) Environ Sci Technol 5:9790–9798
5. Eßer E, Kureti S, Heckemüller L, Todt A, Eilts P, Morawietz T, Friedrich A, Waiblinger W, Hosseiny S, Bunar F (2022) SAE Tech Pap 2022-01-0538
6. Koch DT, Eßer E, Kureti S, Sousa A (2020) MTZ Worldw 81:630–635
7. Pachauri RK, Meyer LA (2014) Climate Change 2014: Synthesis report contribution of working groups I, II and III to the fifth assessment report of the intergovernmental panel on climate change IPCC, p 151
8. Hu Z, Yang RT (2019) Ind Eng Chem Res 58:2410140–2410153
9. Liu Z, Wu J, Hardacre C (2018) Catal Surv from Asia 22:3146–3155
10. Hamada H, Haneda M (2012) Appl Catal A-Gen 421:1–13
11. Liu Z, Li J, Woo SI (2012) Energy Environ Sci 5:108799–108814
12. Eßer E, Schröder D, Nartova AV, Dmitrachkov AM, Kureti S (2022) Catal Lett 152:61598–61610
13. Costa CN, Efstathiou AM (2007) Appl Catal B-Gen 72:3240–3252
14. Chiarello GL, Ferri D, Grunwaldt J-D, Forni L, Baiker A (2007) J Catal 252:2137–2147
15. Liu Z, Lu Y, Yuan L, Ma L, Zheng L, Zhang J, Hu T (2016) Appl Catal B-Gen 188:189–197
16. Schott FJP, Balle P, Adler J, Kureti S (2009) Appl Catal B-Gen 87(1–2):18–29
17. Hahn C, Endisch M, Schott FJP, Kureti S (2015) Appl Catal B-Gen 168:429–440
18. Burch R, Millington PJ, Walker AP (1994) Appl Catal B-Gen 4:165–194
19. Zhang X, Wang X, Zhao X, Xu Y, Liu Y, Yu Q (2015) Chem Eng J 260:419–426
20. Schweicher J, Bundhoo A, Frennet A, Kruse N (2014) Catal Lett 144:2204–2210
21. Acharya CK, Lane AM, Krause TR (2008) Catal Lett 121:112–118
22. Chan D, Gremminger A, Deutschmann O (2013) Top Catal 56:1–8293
23. Green R, Morrall P, Bowker M (2004) Catal Lett 98:2129–2133
24. Jin T, Okuhara T, Mains GJ, White J (1987) J Phys Chem 91:123310–123315
25. Bergeret G, Gallezot P (2008) Particle size and dispersion measurements in handbook of heterogeneous catalysis. Wiley-VCH, Weinheim, pp 738–765
26. Zheng G, Palmer G, Salanta G, Kotrba A (2009) SAE Tech Pap 0148–7191
27. Crocoll M, Kureti S, Weisweiler W (2005) J Catal 229:2480–2489

28. Chatterjee D, Deutschmann O, Warnatz J (2002) Faraday Discuss 119:371–384
29. Hahn C, Endisch M, Kureti S (2017) Top Catal 60:3238–3242
30. Lox ESJ (2008) Automotive exhaust treatment in handbook of heterogeneous catalysis. Wiley-VCH, Weinheim, pp 2274–2345
31. Haynes WM, Lide DR, Bruno TJ (2016) CRC handbook of chemistry and physics. CRC Press, Boca Raton
32. Borchers M, Keller K, Lott P, Deutschmann O (2021) Ind Eng Chem Res 60:186613–186626